Journal of Biomedical Optics

SPIEDigitalLibrary.org/jbo

Optical detection and measurement of living cell morphometric features with single-shot quantitative phase microscopy

Pierre Bon
Julien Savatier
Marine Merlin
Benoît Wattellier
Serge Monneret

SPIE

Optical detection and measurement of living cell morphometric features with single-shot quantitative phase microscopy

Pierre Bon,[a,b] Julien Savatier,[a] Marine Merlin,[a] Benoît Wattellier,[b] and Serge Monneret[a]
[a]Aix-Marseille Université, Ecole Centrale Marseille, CNRS UMR 7249, Institut Fresnel, Marseille, France
[b]Phasics, Xtec Bât 404, Campus Polytechnique, Palaiseau, France

Abstract. We present a quadriwave lateral shearing interferometer used as a wavefront sensor and mounted on a commercial non-modified transmission white-light microscope as a quantitative phase imaging technique. The setup is designed to simultaneously make measurements with both quantitative transmission phase and fluorescence modes: phase enables enhanced contrasted visualization of the cell structure including intracellular organelles, while fluorescence allows a complete and precise identification of each component. After the characterization of the phase measurement reliability and sensitivity on calibrated samples, we use these two imaging modes to measure the characteristic optical path difference between subcellular elements (mitochondria, actin fibers, and vesicles) and cell medium, and demonstrate that phase-only information should be sufficient to identify some organelles without any labeling, like lysosomes. Proof of principle results show that the technique could be used either as a qualitative tool for the control of cells before an experiment, or for quantitative studies on morphology, behavior, and dynamics of cells or cellular components. [DOI: 10.1117/1.JBO.17.7.076004]

Keywords: quantitative phase microscopy; fluorescence; organelles; cell morphology.

Paper 11756 received Dec. 14, 2011; revised manuscript received Jun. 6, 2012; accepted for publication Jun. 14, 2012; published online Jul. 6, 2012.

1 Introduction

Nomarski/differential interference contrast (DIC) microscopy[1] is widely used in biology because of its capability to infer morphometric features even inside transparent samples. It transfers the phase information of the sample into the intensity distribution of the relevant final image. However, the relationship between image intensity contrast level and related sample phase gradient is nonlinear, implying the technique is only qualitative. This probably motivated several groups to develop quantitative phase microscopy over the past decade.

Different approaches have been followed to obtain a quantitative phase. Even though isolated works were based on beam propagation along the optical axis around the focal plane,[2] or more recently on the use of chromatic aberrations,[3] most concerned holographic microscopy. Thus, they used coherent interferometry with a supplementary reference beam that implies a hardware modification of the microscope.[4–6] However, temporally coherent illumination has also been proposed, where measurements were made with systems based on grating[7] or wavefront sensors. Those systems are directly plugged onto a video port of a conventional host bright field microscope and give both intensity and phase of a light wave separately and quantitatively.[8,9] Sampling of the complex electromagnetic field in a reference plane that generally corresponds to the plane where the sensor is placed is thus available.

A key role of phase contrast imaging is that it provides information in the form of local changes in the optical path difference. As a consequence, once a biological sample is concerned, it reveals morphometric features without the need for exogenous molecules like fluorophores. Quantification of the phase even allows extracting important biophysical cell parameters as dry mass,[10–12] optical volume, cell shape, and thus average intracellular refractive index.[13,14] Very recently, it also revealed quantitative parameters linked to cell dynamics,[15] such as intracellular transport[16] or cell growth.[17]

As initially described in Ref. 8, wavefront sensing based on lateral shearing interferometry is particularly suitable for measuring the phase distribution of microscopic samples. As a consequence, it should be useful to detect and measure distinctive parameters of living cells organelles. As opposed to other existing techniques mentioned above, it offers to measure phase and intensity from a single-shot acquisition, with sub-nanometric sensitivity in the optical path difference, diffraction-limited lateral resolution, and under partially coherent illumination. This last point makes the system successful when directly plugged onto a non-modified conventional microscope using its native broadband light source. In this paper, we first present the experimental setup we built to simultaneously image biological samples with both quantitative phase and fluorescence contrasts. We then apply the system to calibrated samples to evaluate the reliability and sensitivity of the technique. Finally, we correlate fluorescence with phase contrast in order to measure optical thickness of specific organelles in living cells.

2 Materials and Methods

2.1 *Lateral Shearing Interferometry*

Lateral shearing interferometry is a technique to measure the phase gradient of a given light wavefront in one direction,

Address all correspondence to: Serge Monneret, Aix-Marseille Université, Ecole Centrale Marseille, CNRS UMR 7249, Institut Fresnel, Marseille, France. Tel: +33 491288052; Fax: +33 491288067; E-mail: serge.monneret@fresnel.fr

0091-3286/2012/$25.00

from its replication into two identical but tilted copies. This offers the key advantage that it works without any use of a reference light beam. More precisely, the incident wavefront is replicated, thanks to a sinusoidal amplitude grating. After a few millimeters propagation, a mutual interference pattern is recorded with a video camera. In the case of a flat incident wavefront, the interference pattern gives regular fringes of period p and hence produces two well-defined spots corresponding to the fringe frequency $1/p$ in the Fourier plane. In the case of an arbitrary wavefront, the interference gives a non-regular interferogram that presents local changes in the fringe spatial frequency with respect to the corresponding phase gradient of the incident beam.

However, reconstruction methods require the wavefront derivatives along two orthogonal directions to avoid error propagation and then to fully recover the actual two-dimensional phase distribution of the incident field. Multiwave interferometry solved the problem by offering a single-shot acquisition of at least two wavefront derivatives.[18] In the particular case of quadriwave lateral shearing interferometry (QWLSI), four replicas are created by a specific two-dimensional diffraction grating, allowing two gradients along two orthogonal directions to be measured and then integrated to determine both the intensity and phase of the incident field.[19] As for one-dimensional lateral shearing interferometry, one could use a sinusoidal two-dimensional amplitude grating to generate the four required replicas. In practice, the so-called Modified Hartmann Mask is preferably used because of its much simpler fabrication process: it is an only 3-level amplitude component that has been optimized to diffract more than 90% of the light energy into the selected replicated wavefronts, by properly choosing the ratio between the size of the square holes and the pitch of the mask.[20] Phase gradients are recovered in the Fourier space, by means of a deconvolution around the nominal interferogram fringe frequency $1/p$. Unlike classical interferometers, where a coherent reference arm is mandatory, lateral shearing interferometry is self-referenced, making it particularly insensitive to environmental vibrations, and achromatic.[8] The wavefront sensor we used was a QWLSI commercially available product that has been specifically optimized for biological applications (SID4Bio, Phasics S.A., France). Such a model gives 300×400 phase and intensity measurement points with a lateral pitch of 29.6 μm in the image plane.

2.2 *Experimental Setup*

Combination of phase and epifluorescence imaging is generally interesting because of the complementary information the two

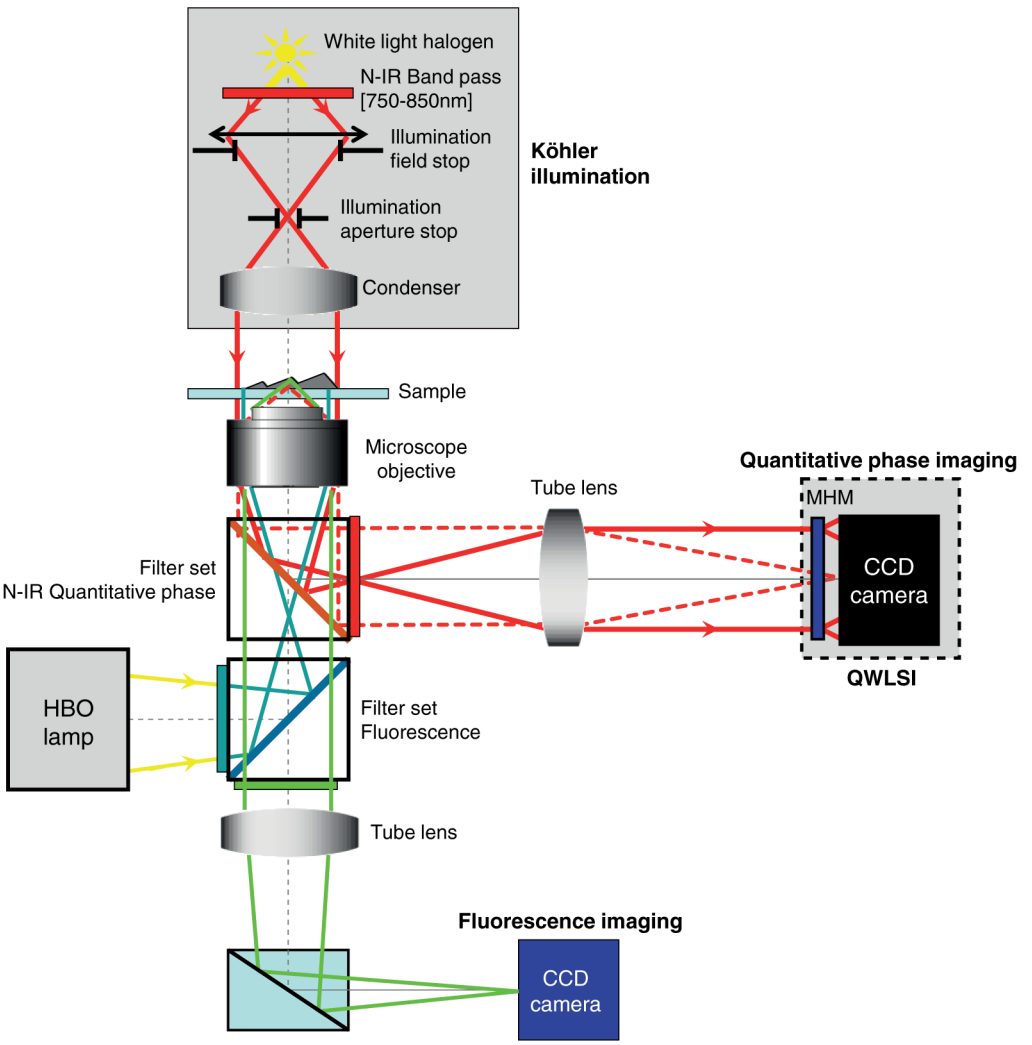

Fig. 1 Schematic layout of the setup.

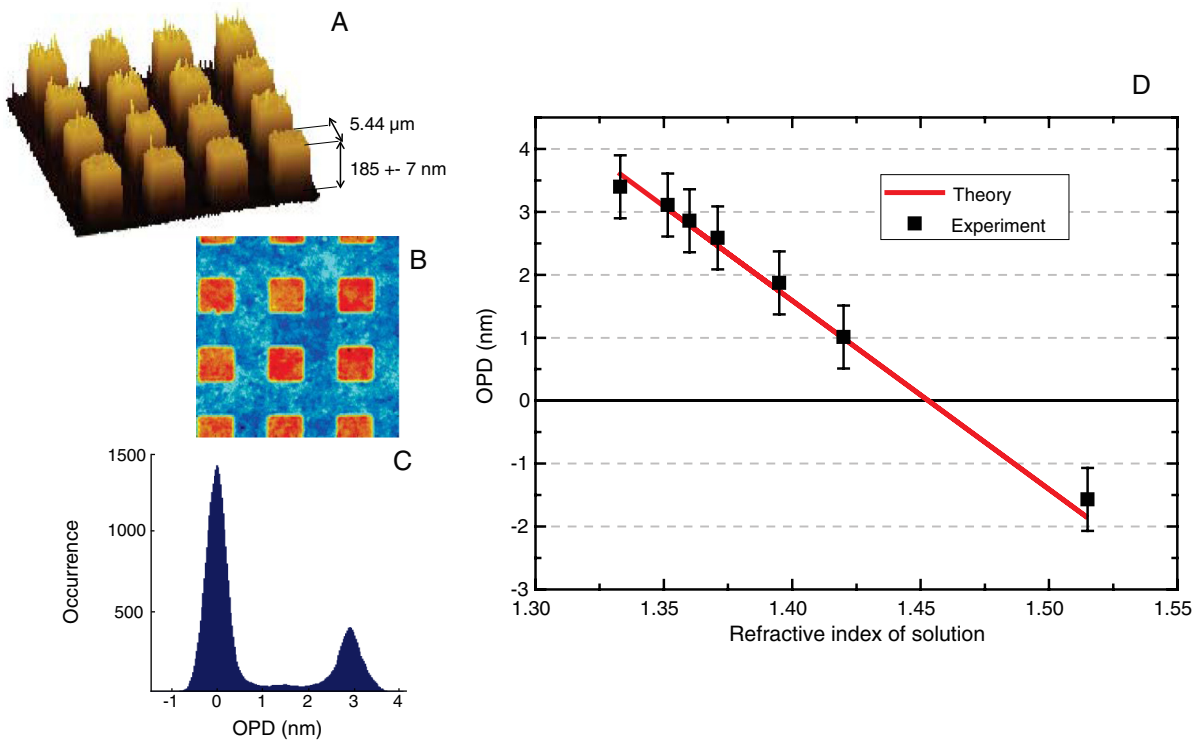

Fig. 2 Measurements on a calibrated etched fused silica sample. (a) Topographic measurement by atomic force microscopy; (b) quantitative OPD map of the sample; (c) histogram of OPD values on each pixel of image (b); and (d) comparative results between theoretical and experimental OPD of the sample in several solutions with different refractive indices. Scale bar: 10 μm.

modalities can offer. Optical path differences (OPD) provide structural information, while fluorescence reveals specific functional parameters about the biological system. Some works combining phase and fluorescence imaging have already been reported.[21,22] Here we used fluorescence in order to specifically identify sub-cellular compartments.

Figure 1 shows the experimental setup we used. The wavefront sensor substituted for a conventional camera plugged into a conventional inverted microscope equipped with a standard broadband halogen lamp as its light source. The microscope (Eclipse TiU, Nikon, Japan) also included an expanded space stratum structure providing an additional back port combined with a second fluorescence filter turret. That is how simultaneous quantitative transmission phase imaging and epifluorescence imaging was performed. A 750 ± 20 nm band-pass filter was added on the transmission illumination path before the sample in order to illuminate it in wide field with near infrared (N-IR) light. The upper filter turret carried a high-pass dichroic filter, reflecting light from 725 nm to around 1 μm and allowing light transmission from 350 to 725 nm. The second filter turret carried conventional fluorescence filter cubes to allow multimarker fluorescence imaging. The QWLS interferometer was plugged onto the microscope back exit port to measure the exit wavefront on the image plane in the N-IR spectral band. A cooled intensity camera (DX2, Kappa opto-electronics GmbH, Gleichen, Germany) was plugged into one of the lateral microscope video port to record fluorescence coming from the sample. A 720 nm short-pass filter was added just before this camera to filter N-IR light that could remain. The two sensors were trigged to measure the fluorescence and the phase signal at the same time. In order to merge phase and fluorescence information and thus to obtain composite phase/fluorescence images, a calibration relative to residual tilt, lateral misplacement and differential magnification between the two sensors was required. An algorithm was then applied to extract the exact position, angle, and dilation of the phase image compared

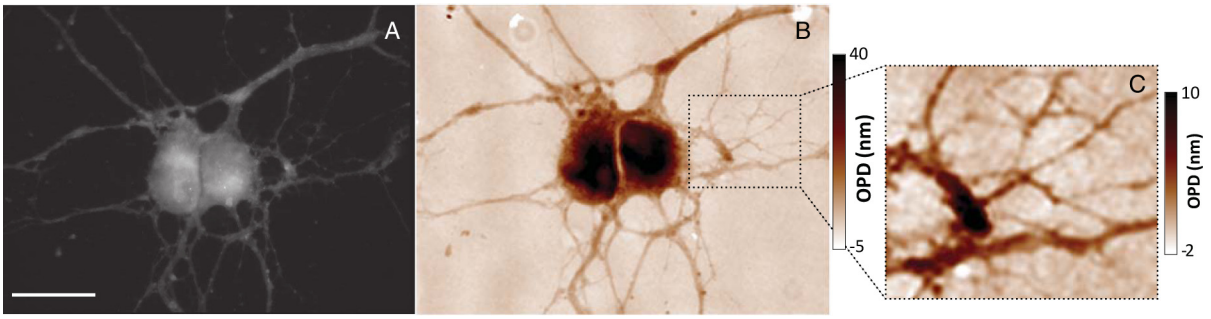

Fig. 3 Fixed human neurons images. (a) Green fluorescent protein (GFP) fluorescence; (b) raw QWLSI phase contrast image; and (c) high-pass filtered sub-image with lookup table saturation to provide enhanced useful contrast. (40×, N.A. 1.3.) Scale bar: 10 μm.

to the fluorescence one. In order to be fully diffraction-limited on the QWLSI sensor, we replaced the back tube lens (400 mm instead of 200). Consequently, the final magnification was 200 in phase for a 100× objective, and still 100 in fluorescence.

The typical irradiance of transmitted light at the sample plane was less than 5 $nW/\mu m^2$ for all the measurements presented in the manuscript. This level of exposure allowed for non-invasive continuous live-cell imaging over extended periods of time in the hour-level range. Fluorescence excitation was automatically cut between acquisitions to avoid photobleaching.

2.3 *Quantitative Phase Measurement Procedure*

Let us define first the optical path difference (OPD) as

$$\mathrm{OPD}(x, y) = \int_0^t \Delta n \mathrm{d}z, \tag{1}$$

where Δn is the change in the refractive index of the sample with respect to that of the surrounding medium, z is the coordinate along the optical axis, and t is the thickness of the sample. In the case where an aberration-free microscope with a flat wavefront illumination is used, the measured phase is the OPD induced by the sample, on the condition that the sample is properly imaged onto the sensing element of the wavefront sensor. In reality, both the non-perfect microscope and non-planar illumination wavefront cause the measured OPD to be the sum of the target phase-shift due to the sample with an additional static phase-shift, which is due to non-optimal optical path inside the system. Yet a simple way to produce direct single-shot phase maps of the actual sample is to measure the static phase-shift distribution from an element-free region of the sample, and to use it as a reference wavefront that will be subtracted from all subsequent phase measurements in order to remove the static OPD.

Once the quantitative phase information is obtained as described above, it is possible to post-process the actual phase image with the help of different types of numerical filters in order to enhance the phase contrast of target details. Typically, high-pass filtering in the spatial frequency domain is an interesting filter as it removes low-frequency information (global shape of the cell, nucleus) and increases the relative dynamics of much smaller details (organelles and membrane ruffles for example). High-pass filtering is tunable and does not present any decrease in the lateral resolution, but it does, of course, modify the global value of the local phase distribution and introduces artifacts. As a consequence, it must be banished in the case of quantitative measurements.

2.4 *Biological Samples and Models*

In this paper, we mostly used COS-7 cells, adherent African green monkey kidney fibroblast-like cells. They are particularly interesting for studying membrane dynamics and intracellular movements.[23] They are also easy to transduce. They were seeded in a 2-well Lab-Tek (Nunc, Roskilde, Denmark) and transduced with CellLight reagents (Life Technologies, Saint Aubin, France) the day before experiment in order to specifically label given organelles with fluorescent fusion proteins.

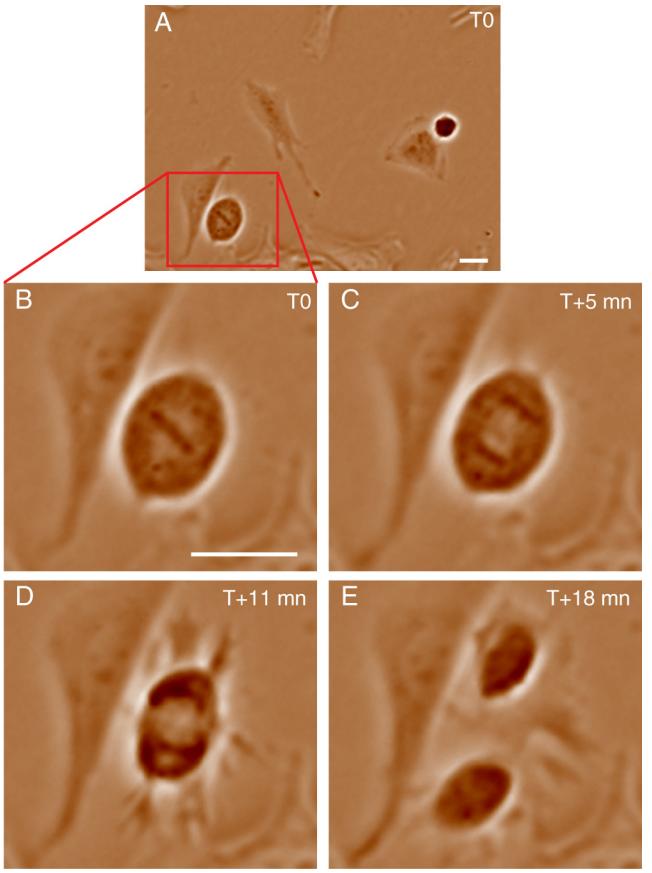

Fig. 4 Sequence of filtered QWLSI phase images recorded during HeLa cells mitosis. (a) Full field image, and (b) to (e) zoom on the cell of interest. (b) Metaphase, (c) anaphase, (d) telophase, and (e) cytokinesis. (40×, N.A. 1.3.) Scale bars: 20 μm.

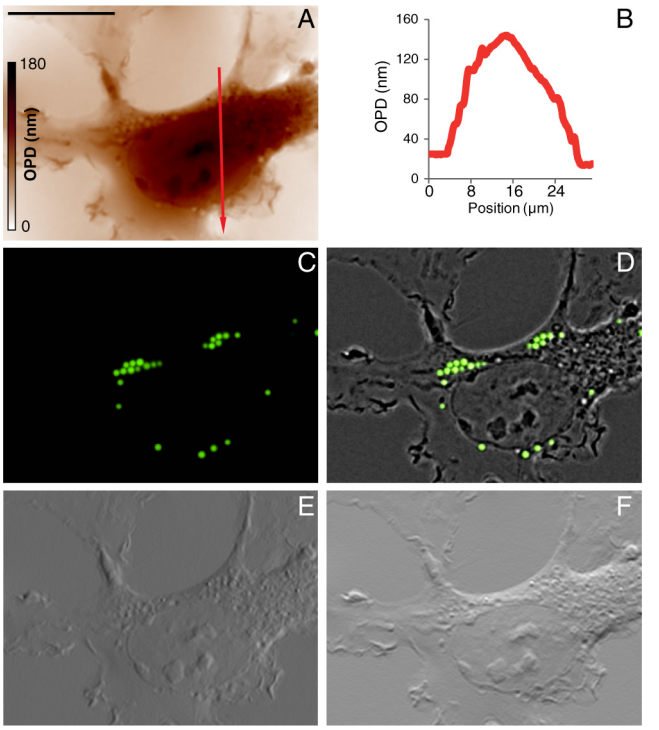

Fig. 5 Different ways to use QWSLI images to look at a COS-7 cell. (a) Quantitative phase image with a phase level sectioning (red arrow). (b) Result of this sectioning showing a really good SNR. (c) Fluorescence image of peroxysomes obtained simultaneously with a video camera, combined in (d) with filtered phase image. (e) and (f) simulated post processing DIC images from a single acquisition along two perpendicular axes [(e) 0° and (f) 90°]. (100×, N.A. 1.3.) Scale bar: 10 μm.

Imaging and cell cultures were done in Dulbecco's Modified Eagle Medium, supplemented with 5% fetal calf serum and sodium pyruvate. For long imaging experiments, cells were placed in a 37 °C box over the microscope, with a small incubation chamber providing humidified air with 5% carbon dioxide.

We also used a periodical microstructured etched fused silica glass as a model solid sample. Surface topography was determined by atomic force microscopy [Fig. 2(a)], showing an etching depth of 30 nm. The refractive index of the fused silica used (ACM, France) was 1.453 around the 770 nm central wavelength of the measurement beam.

3 Results

3.1 *Quantitative Phase Imaging on a Calibrated Model*

In order to characterize resolution and reliability of our system, we first tested it on solid calibrated structures. They were embedded in liquid media with known but varying refractive indices and could work as a model of biological features of interest. More precisely, we successively measured the OPD image of our silica model sample when embedded in different liquid media (pure water, water with varying glucose concentration, and immersion oil), with known refractive indices determined, thanks to an Abbe refractometer (2WAJ, HuiXia Supply, China). Figure 2(d) shows the highly coherent results that we obtained when comparing the theoretical OPD given by Eq. (1) with the experimental data. Such an experiment also enables us to determine the noise level: Fig. 2(b) gives the OPD map as measured, and Fig. 2(c) gives its OPD histogram. The sharpness of this histogram leads us to define the error bars of Figure 2(d) as ±0.5 nm. Full width half maxima of the two histogram peaks also give ±0.5 nm as the typical noise level in the OPD images.

3.2 *Optical Detection of Cellular Features*

Fixed human neurons have been imaged (Fig. 3) in order to show that QWLSI is a well-adapted tool to detect and observe thin membrane filaments, by exhibiting a contrast that is comparable to that obtained with fluorescence imaging. The advantage of the phase technique is that it does not require fluorescence labeling that can be saved for functional imaging.

Another interesting point of phase contrast microscopy is that one can detect subcellular features as soon as they present a refractive index that slightly differs from that of the cytosol. In that case, using high-pass filtering in the spatial frequency domain of phase images increases the resulting contrast and therefore enables the clear detection of the target features. As an example, Fig. 4 shows an 18-min long sequence of filtered QWLSI phase images of a HeLa cell mitosis, revealing different phases of the cell-division cycle. In Fig. 4(b), the cell is in metaphase, where spindle fibers align chromosomes in the middle of the cell, along the metaphase plate. Figure 4(c) shows anaphase, where chromatids separate and move to opposite sides of the cell. Figure 4(d) corresponds to telophase, where chromatids arrive at the opposite poles and new membranes form around the daughter nuclei. Finally, cytokinesis appears [Fig. 4(e)], where two daughter cells are now individualized.

3.3 *Quantitative Phase Imaging on Biological Samples*

We now present different ways to study living cells from quantitative OPD images obtained with the QWLSI technique.

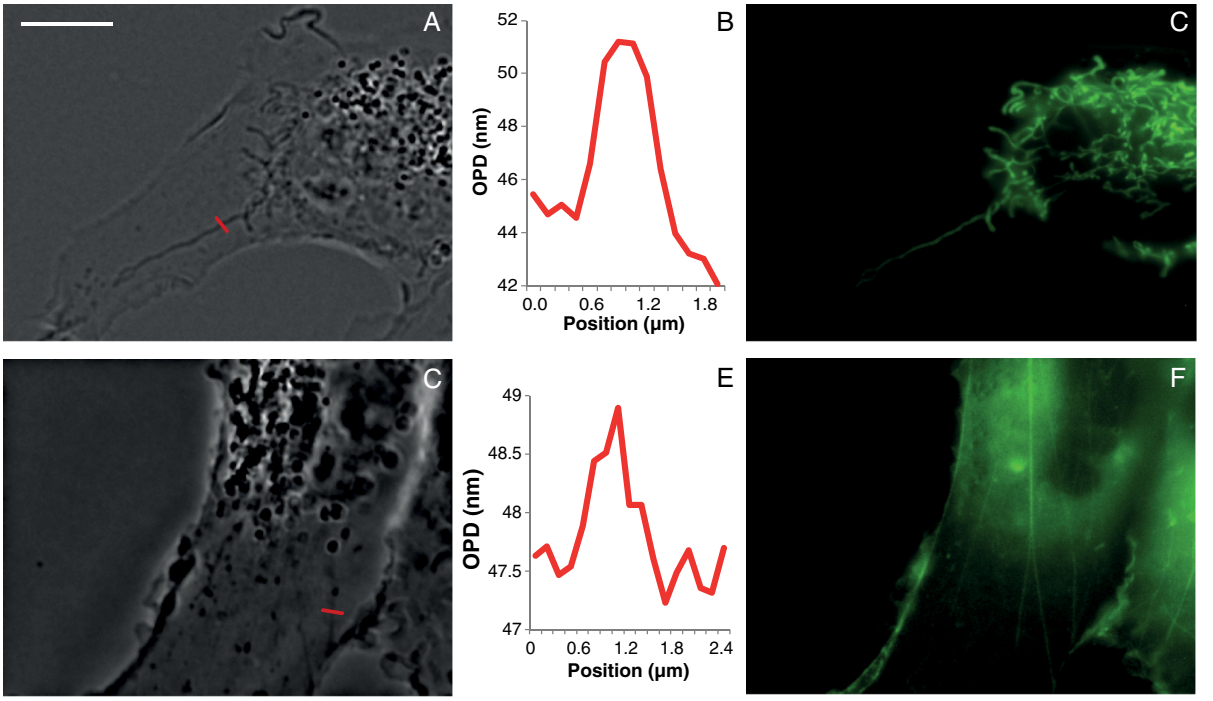

Fig. 6 Quantitative phase measurement in COS-7 cells. (a), (b), and (c) Mitochondria tubular network focusing. (d), (e), and (f) Actin stress fiber focusing. (a) and (d) High-pass filtered phase image with phase level sectioning (red lines). (b) and (e) Phase level sectioning along the red lines defined in (b) and (d) but from raw images (not shown). (c) and (f) Simultaneous GFP fluorescence images, needed to localize labeled organelles. (100×, N.A. 1.3.) Scale bar: 10 μm.

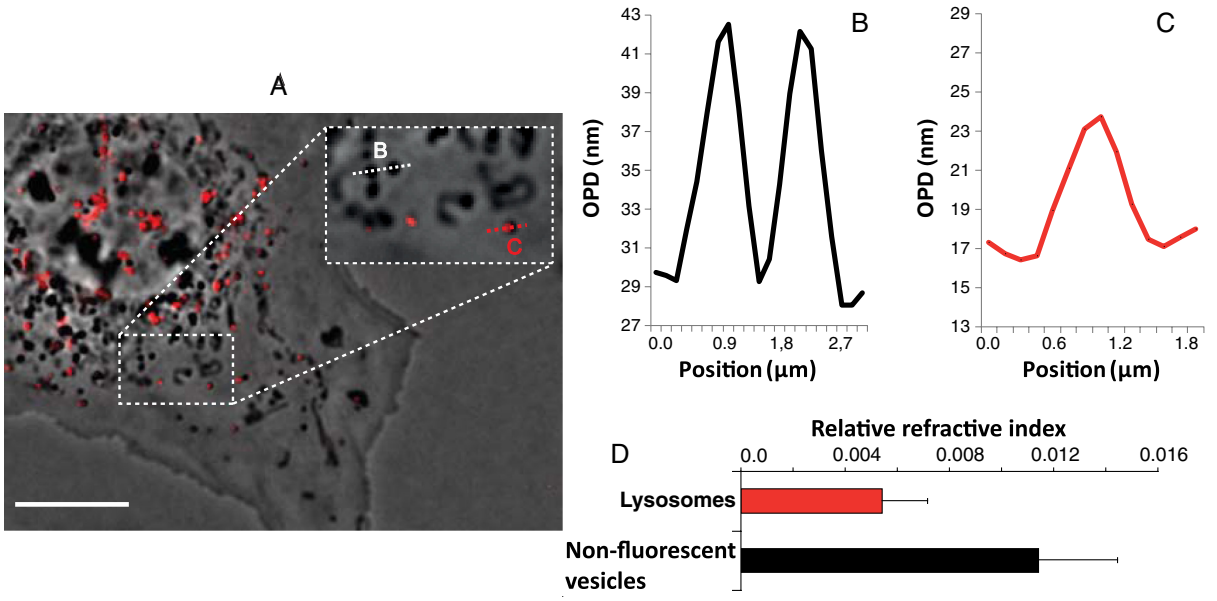

Fig. 7 Quantitative phase measurement of lysosomes compared to others vesicles, in COS-7 cells. (a) An example of composite phase/fluorescence images (red: RFP, lysosomes), with a zoomed insert (b). (c) and (d) Phase level sectioning of vesicles along the red and white dotted lines drawn in (b). (e) Relative refractive index (Δn/diameter) distribution of fluorescent lysosomes and other non-fluorescent vesicles (average values and standard deviation are drawn), obtained from 70 measurements on independent vesicles of around 1-μm diameter, showing a significant difference between the two populations.

With the quantitative raw image of Fig. 5(a), we measured OPD in different parts of a COS-7 cell with a high signal to noise ratio [SNR; Fig. 5(b)]. We also combined fluorescence and high-pass filtered phase images, simultaneously, to detect specific organelles in real time, as for peroxysomes [Fig. 5(c) and 5(d)]. Additionally, we simulated DIC images by simply calculating the gradient of the OPD map in a given direction [Fig. 5(e) and 5(f)], thanks to its quantitative artifact-free nature.

Figure 6 shows experimental results obtained with transiently transduced COS-7 cells that expressed fusion proteins specific of mitochondria or actin (CellLight, Invitrogen). Observations were made with a 100×, NA = 1.3 immersion objective in order to visualize a single cell with a good lateral resolution. Post-processing high-pass filtering was used to increase the phase contrast of target organelles, such as mitochondria, actin stress fibers, or vesicles [Figs. 6(a), 6(d), and 7, respectively]. However, as described in Sec. 2.3, OPD measurements were made on raw images.

Mitochondria are not always individualized, but can form a tubular network [Fig. 6(a) and 6(c)]. Identification of mitochondria can be achieved by using morphological criterion on OPD images. Relative OPD of tubular and horizontal mitochondria (compared to the cell background) is quite constant in a given cell [about 6 nm for a diameter of 1.2 μm, see Fig. 6(b)]. Nevertheless, we are unable to quantify OPD of a specific organelle in very dense area, such as the perinuclear zone, where the endoplasmic reticulum and Golgi apparatus are located. We did not detect clear individual mitochondrion in our cells, neither in fluorescence nor in phase.

We then applied the technique to a cytoskeleton study. Actin stress fibers are made of many polymers of actin and are synthesized by the cell in order to keep its structure and to move on the surface [Fig. 6(f)]. Though monomeric actin is not big and dense enough to be seen with our technique, its polymeric form can be detected with the actual setup [Fig. 6(d)]. Figure 6(e) shows an OPD of around 1.5 nm for the biggest fibers, close to the sensitivity limit of the technique (SNR = 3).

Figure 7 demonstrates the possibility of determining specific vesicles by only using the quantitative phase-contrast technique. We indeed labeled lysosomes on COS-7 cells with red fluorescent protein fusion proteins [Fig. 7(a)], and measured 32 fluorescent lysosomes and 38 other non-fluorescent vesicles of similar diameters, taken from five different living COS-7 cells [examples in Fig. 7(b) and 7(c)]. The results [Fig. 7(d)] clearly present two significantly different vesicles groups with respect to their relative refractive index Δn, where Δn is the difference between the refractive index of the considered vesicle and that of the surrounding medium. Reaching Δn was possible by assuming the vesicles were both homogeneous and spherically shaped, which is often but not always the case.

4 Conclusions

For samples that present both a small thickness and a weak refractive index contrast with their environmental medium, one can consider that the OPD measured by the system is the real one.[8] In case of higher thickness or higher refractive index contrast, one can observe appreciable difference between experimental measurements and real OPD, because the real image formation process includes both diffraction due to the sample and optical properties of the actual imaging system.

In this paper, we only considered a weak diffraction regime to interpret measurements relative to biological samples. Experiments with the calibrated silica sample demonstrate that this assumption is clearly valid with features that are fully in the depth of focus and present OPD of a few nanometers. Moreover, the N-IR band-pass filter placed on the transmission illumination path prevents it from working in the absorption spectral band of a labeled biological sample where its refractive index could change appreciably. As a consequence, we always considered that OPD was simply described by Eq. (1) in this paper.

We then demonstrated that QWLSI is a very simple and well-adapted tool to produce quantitative values of phase-shift introduced by a sample. One key issue of the technique is that it only requires a camera-like sensor. This implies that it can be used on most of conventional full-field microscopes, without modifying their light path. Moreover, it gives highly contrasted phase images with no specific sample preparation, even if fluorescence images often have better contrast.

We first applied the technique to check cell morphology, which is closely related to the living state of the cells that are studied. One simple way to verify that living cells are in good condition is to visualize the cell membrane shape, with particular interest on the leading edge of lamellipodia and on microspikes. QWLSI seems to be particularly efficient for this specific but important monitoring. We next presented characteristic phase-shifts of specific subcellular elements like mitochondria or vesicles and also measured an OPD of around 1.5 nm for the biggest actin fibers in our COS-7 cells, close to the sensitivity limit of the technique. Such detection without labeling should be very interesting when applied to cell movement.

This technique should also be of interest in locating a specific target area in a specimen, thanks to its non-destructive contrast enhancement. Then, combination with fluorescence microscopy, without relocating the specimen, would offer functional imaging for molecular interactions or dynamics experiments. The major advantage would be to minimize problems due to photobleaching and to save one or more colors for highly specific studies. In the future, QWLSI should be used for the quantitative analysis of specific organelles during creation or dynamics analysis (especially vesicles), since intracellular segmentation should be clearly simplified by the free-halo and highly contrasted resulting images.

Finally, DIC simulation was demonstrated, as it should be useful for biologists who are used to looking at their samples with this well-established technique. Specific interest here is that one can tune both the angle and the contrast level, during acquisition or as a post-acquisition numerical process.

Acknowledgments

The authors would like to thank Didier Marguet (Centre d'Immunologie de Marseille Luminy) for fruitful discussions. Calibrated etched fused silica samples were manufactured and characterized by atomic force microscopy in the "Laboratoire Hubert Curien" (Saint-Etienne, France) under the responsibility of Pierre Pommier. This work was supported by the French "Fonds Unique Interministériel," through the "QUITO" project, also involving the "Conseil Régional Région Provence Alpes Côte d'Azur." The authors would also like to thank the CNRS research network "GDR 2588" devoted to functional imaging and microscopy for fruitful discussions and collaborations. *Conflict of interest*: The authors declare the following competing financial interest: Phasics company is the supplier of the QWLSI system that is the key-element of the technique described in this paper.

References

1. G. Nomarski, "Nouveau dispositif pour l'observation en contraste de phase différentiel," *J. Phys. Radium* **16**(5), S88–S88 (1955).
2. A. Barty et al., "Quantitative optical phase microscopy," *Opt. Lett.* **23**(11), 817–819 (1998).
3. L. Waller et al., "Phase from chromatic aberrations," *Opt. Express* **18**(22), 22817–22825 (2010).
4. E. Cuche, P. Marquet, and C. Depeursinge, "Simultaneous amplitude-contrast and quantitative phase-contrast microscopy by numerical reconstruction of Fresnel off-axis holograms," *Appl. Opt.* **38**(34), 6694–7001 (1999).
5. D. Carl et al., "Parameter-optimized digital holographic microscope for high-resolution living-cell analysis," *Appl. Opt.* **43**(36), 6536–6544 (2004).
6. P. Marquet et al., "Digital holographic microscopy: a noninvasive contrast imaging technique allowing quantitative visualization of living cells with subwavelength axial accuracy," *Opt. Lett.* **30**(5), 468–470 (2005).
7. D. Fu et al., "Quantitative DIC microscopy using an off-axis self-interference approach," *Opt. Lett.* **35**(14), 2370–2372 (2010).
8. P. Bon et al., "Quadriwave lateral shearing interferometry for quantitative phase microscopy of living cells," *Opt. Express* **17**(15), 13080–13094 (2009).
9. X. Cui et al., "Wavefront image sensor chip," *Opt. Express* **18**(16), 16685–16701 (2010).
10. R. Barer, "Interference microscopy and mass determination," *Nature* **169**(4296), 366–367 (1952).
11. G. Popescu et al., "Optical imaging of cell mass and growth dynamics," *Am. J. Physiol.: Cell Physiol.* **295**(2), C538–C544 (2008).
12. B. Rappaz et al., "Noninvasive characterization of the fission yeast cell cycle by monitoring dry mass with digital holographic microscopy," *J. Biomed. Opt.* **14**(3), 034049 (2009).
13. B. Rappaz et al., "Measurement of the integral refractive index and dynamic cell morphometry of living cells with digital holographic microscopy," *Opt. Express* **13**(23), 9361–9373 (2005).
14. B. Kemper et al., "Integral refractive index determination of living suspension cells by multifocus digital holographic phase contrast microscopy," *J. Biomed. Opt.* **12**(5), 054009 (2007).
15. G. Popescu et al., "Fourier phase microscopy for investigation of biological structures and dynamics," *Opt. Lett.* **29**(21), 2503–2505 (2004).
16. P. Wang et al., "Dispersion-relation phase spectroscopy of intracellular transport," *Opt. Express* **19**(21), 20571–20579 (2011).
17. M. Mir et al., "Optical measurement of cycle-dependent cell growth," *PNAS* **108**(32), 13124–13129 (2011).
18. J. Primot and L. Sogno, "Achromatic three-wave (or more) lateral shearing interferometer," *J. Opt. Soc. Am. A* **12** (12), 2679–2685 (1995).
19. S. Velghe et al., "Wave-front reconstruction from multidirectional phase derivatives generated by multilateral shearing interferometers," *Opt. Lett.* **30** (3), 245–247 (2005).
20. J. Primot and N. Guérineau, "Extended Hartmann test based on the pseudoguiding property of a Hartmann mask completed by a phase chessboard," *Appl. Opt.* **39** (31), 5715–5720 (2000).
21. Y. Park et al., "Diffraction phase and fluorescence microscopy," *Opt. Express* **14**(18), 8263–8268 (2006).
22. N. Pavillon et al., "Cell morphology and intracellular ionic homeostasis explored with a multimodal approach combining epifluorescence and digital holographic microscopy," *J. Biophotonics* **3**(7), 432–436
(2010).
23. A. Sergé et al., "Dynamic multiple-target tracing to probe spatiotemporal cartography of cell membranes," *Nat. Methods* **5**(8), 687–694 (2008).